Estimation of Cyclable Lithium for Li-ion Battery State-of-Health Monitoring

Saehong Park, Dong Zhang, Reinhardt Klein, Scott Moura

Abstract-State of health (SOH) estimation for Li-ion batteries enables high-fidelity monitoring and high-performance in advanced battery management systems for applications such as mobile devices, electrified transportation, and energy storage. In order to achieve accurate SOH information, this paper improves the output voltage prediction by considering state-dependent parameters for a reduced-order electrochemical model. In addition, the SOH information is defined as the total moles of lithium in both solid-phase and electrolyte-phase, which directly affects the initial conditions of the electrochemical states in the model. We validate that the change of these parameters leads to capacity fade and power fade in terms of battery life cycling. The sensitivity equations are derived for these SOH parameters, and used to track the parameter changes via gradient-based parameter fitting algorithm. Simulation results demonstrate the proposed SOH estimation scheme using voltage and current measurements.

I. INTRODUCTION

This paper examines estimation of lithium in the solid-phase and electrolyte-phase of electrochemical battery models, for state-of-health estimation.

With the evolution of electrified transportation and smart grid, lithium-ion (Li-ion) batteries have emerged as one of the leading energy storage sources, due to their high energy density [1]. An advanced battery management system (BMS) executes real-time estimation and control algorithms to ensure battery safety and efficient operations. One of the crucial functionalities of BMS is to estimate the state of charge (SOC) and state of health (SOH), and ultimately construct optimal energy management strategies.

Model-based estimation for Li-ion batteries has been widely studied in the literature [2]. There are two mainstream battery modeling frameworks, one is the equivalent circuit models (ECMs), and the other one is electrochemical models. ECMs have simple structures to represent the input-output behavior of batteries by using circuit elements such as resistors and capacitors [3]. However, ECMs do not directly represent certain physical phenomena of batteries, namely capacity fade, lithium plating, and other degradation mechanisms, which are specific electrochemical, mechanical, and/or thermal processes. The second category is electrochemical models which account for diffusion, intercalation, and electrochemical kinetics [4]. The mathematical structure is formulated as nonlinear partial

This work was supported by the National Science Foundation under Grant No. 1847177.

S. Park, D. Zhang, and S. Moura are with the Department of Civil and Environmental Engineering, University of California, Berkeley, CA 94720, USA ({sspark,dongzhr,smoura}@berkeley.edu).

R. Klein is with the Robert Bosch LLC, Research and Technology Center, Palo Alto, CA 94304 USA reinhardt.klein@us.bosch.com.

978-1-6654-4197-1/\$31.00 ©2021 AACC

differential equations (PDEs) – ordinary differential equations (ODEs) coupled with algebraic equations. Although these models can precisely explain the internal behavior of the battery, this creates system observability [5], [6] and identifiability issues [7], [8] for battery management system.

Electrochemical models are often reduced in complexity to balance prediction accuracy with a control-oriented structure that enables online algorithm design. The simplest electrochemical model is single particle model (SPM) where a single particle replaces the spatial distribution of active particles in each electrode, and the electrolyte concentration is treated as constant in space and time. State estimation based on SPM is conducted by using a Kalman filter in [9], [10]. Furthermore, nonlinear and backstepping state estimation techniques based on the SPM can be found in [11], [12]. The limitation of SPM is that it neglects the electrolyte dynamics, which play an important role during high charge and discharge events. For this reason, researchers consider SPM with electrolyte dynamics (SPMe) to understand the internal behavior more accurately than SPM. The authors in [13] derived SPMe by using asymptotic methods to reduce the full-order model to simpler forms. A state-of-the-art backstepping state estimation approach based on SPMe can be found in [14]. Tanim et al. [15] augments the SPMe with Arrhenius relations for the model parameters to account for temperature variation, abbreviated as SPMeT. In addition, the author uses Luenberger state estimator based on this model [16]. While SOC estimation can be considered as a state estimation design problem, the SOH estimation problem is not clearly defined. There are many aging mechanisms to describe degradation [17], and they can be difficult to integrate with the electrochemical models and validate experimentally.

SOH estimation for electrochemical models is still a nascent research topic in the literature. One of the most dominant sources for the loss of cell capacity is the loss of cyclable lithium induced by anodic solid-electrolyte interphase (SEI) layer growth [18], [19]. SEI layer growth was found to be the dominant cause of capacity fade during the first 200 cycles (also known as the acceleration stage) [20]. Side reactions, such as SEI layer growth and lithium plating/striping, can alter the amount of lithium/lithium-ions in either the solid-phase $(n_{Li,s})$ or electrolyte-phase $(n_{Li,e})$. Many previous works have addressed capacity estimation by tracking model parameters [21], [22], [23], but very few have focused on battery SOH estimation by estimating the moles of cyclable lithium. Previously, an adaptive PDE observer coupled with a least-squares algorithm was proposed to identify solid-phase lithium as well as internal resistance [24]. The extended Kalman filter (EKF)

was also employed to estimate the amount of cyclable Liions as an unknown model parameter using a single particle model [25]. In [26], the total number of lithium in solid-phase in a reduced SPM was estimated though estimation of the states. Although these works illuminate the importance of cyclable lithium, none of the aforementioned literature (i) simultaneously estimates solid-phase and electrolyte-phase lithium, and (ii) mathematically analyzes the sensitivities of these two parameters to the output voltage.

In light of the previously highlighted works, this paper addresses these challenges by proposing a parameter estimation framework driven by parameter sensitivity analysis for a reduced-order electrochemical model. In particular, this work is motivated by the authors' previous work [24], [14], [7]. First, we improve the output voltage prediction accuracy by considering state-dependent parameters, i.e. conductivity and the activity coefficient in the electrolyte dynamics. The performance of the proposed reduced-order model is demonstrated by comparing it against a full-order model and the previous reduced-order model in [14]. Secondly, we formulate the SOH estimation problem as a parameter estimation of cyclable lithium in both the solid-phase and electrolyte-phase of an electrochemical model. Drifting SOH parameters leads to voltage deviations compared to a fresh cell, which imply capacity and power fade. Lastly, we construct a parameter estimation scheme using sensitivity analysis that exploits the choice of cyclable lithium as the unknown parameters. We verify the proposed parameter estimation technique in the simulation.

The remainder of the paper is organized as follows. Section II derives the single particle model with electrolyte coupled with state-dependent model parameters, and performs model comparison with DFN and conventional SPMe. Section III analyzes parameters' local sensitivities and proposes a nonlinear optimization problem for parameter identification. Section IV demonstrates numerical performance of the proposed estimation scheme. Conclusions are discussed in Section V.

II. ELECTROCHEMICAL MODELS

In this section, we introduce a single particle model with electrolyte dynamics (SPMe) from the full-order model, also known as the Doyle-Fuller-Newman (DFN) model. The full-order model is briefly introduced to derive the SPMe model, and the model reduction procedure is presented along with a graphical comparison.

A. The Full-Order Electrochemical Model

The DFN model consists of two electrically separated porous electrodes and a separator, as shown in Fig. 1. The lithium ions are transported by a diffusion process inside the active particles along the r-axis in the solid phase. They traverse the particle-electrolyte interface via Butler-Volmer kinetics. The ions dissolved in the electrolyte pass through the separator to the opposite electrode along the x-axis. The diffusion, intercalation, and electrochemical kinetics account for the internal battery dynamics expressed by a combination of partial differential equations (PDEs) and ordinary

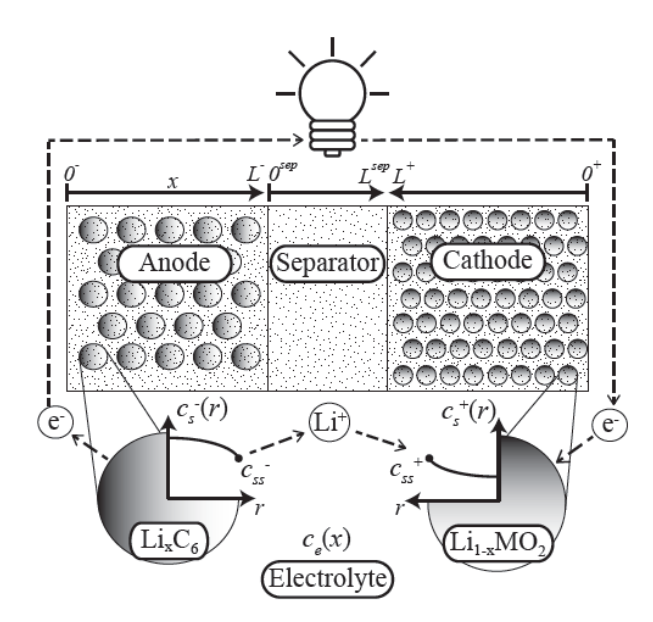


Figure 1: Schematic of the Doyle-Fuller-Newman model [27].

differential equations (ODEs). The state variables are lithium concentration in the solid $c_s^\pm(x,r,t)$, lithium concentration in the electrolyte $c_e(x,t)$, solid electric potential $\phi_s^\pm(x,t)$, electrolyte electric potential $\phi_e(x,t)$, ionic current in the electrolyte $i_e^\pm(x,t)$, and molar ion fluxes between electrodes and electrolyte $j_n^\pm(x,t)$. We summarize the governing equations for $j \in \{-, \text{sep}, +\}$,

$$\frac{\partial c_s^{\pm}}{\partial t}(x,r,t) = \frac{1}{r^2} \frac{\partial}{\partial r} \left[D_s^{\pm} r^2 \frac{\partial c_s^{\pm}}{\partial r}(x,r,t) \right], \tag{1}$$

$$\varepsilon_e^j \frac{\partial c_e^j}{\partial t}(x,t) = \frac{\partial}{\partial x} \left[D_e^{\text{eff}}(c_e^j) \frac{\partial c_e^j}{\partial x}(x,t) + \frac{1 - t_c^0}{F} i_e^j(x,t) \right], \tag{2}$$

$$\sigma^{\text{eff},\pm} \cdot \frac{\partial \phi_s^{\pm}}{\partial x}(x,t) = i_e^{\pm}(x,t) - I(t), \tag{3}$$

$$\kappa^{\text{eff}}(c_e) \cdot \frac{\partial \phi_e}{\partial x}(x,t) = -i_e^{\pm}(x,t) + \kappa^{\text{eff}}(c_e) \frac{2RT}{F} (1 - t_c^0)$$

$$\times \left(1 + \frac{d \ln f_{c/a}}{d \ln c_e}(x,t) \right) \frac{\partial \ln c_e}{\partial x}(x,t), \tag{4}$$

$$\frac{\partial i_e^{\pm}}{\partial x}(x,t) = a_s^{\pm} F j_n^{\pm}(x,t), \tag{5}$$

$$j_n^{\pm}(x,t) = \frac{1}{F} i_0^{\pm}(x,t) \left[e^{\frac{\alpha_a F}{RT} \eta^{\pm}(x,t)} - e^{-\frac{\alpha_c F}{RT} \eta^{\pm}(x,t)} \right], \quad (6)$$

where $t\in\mathbb{R}_+$ represents time. Note that electrolyte-phase parameters, such as $D_e,\kappa,f_{c/a}$ are functions of the electrolyte concentration. $D_e^{\mathrm{eff}}=D_e(c_e)\cdot(\varepsilon_e^j)^{\mathrm{brug}}$ and $\kappa^{\mathrm{eff}}=\kappa(c_e)\cdot(\varepsilon_e^j)^{\mathrm{brug}}$ are the effective electrolyte diffusivity and effective electrolyte conductivity given by the Bruggeman relationship as well as $f_{c/a}=f_{c/a}\left(c_e(x,t)\right)$ is the activity coefficient. In (6), the exchange current density $i_0^\pm(x,t)$ and over-potential $\eta^\pm(x,t)$ are expressed:

$$i_0^{\pm}(x,t) = k^{\pm} \left[c_{ss}^{\pm}(x,t) \right]^{\alpha_c} \left[c_e(x,t) \left(c_{s,\text{max}}^{\pm} - c_{ss}^{\pm}(x,t) \right) \right]^{\alpha_a},$$

$$\eta^{\pm}(x,t) = \phi_s^{\pm}(x,t) - \phi_e(x,t) - U^{\pm}(c_{ss}^{\pm}(x,t))$$
(7)

$$-FR_f^{\pm}j_n^{\pm}(x,t),\tag{8}$$

where c_{ss} is the solid phase surface concentration $c_{ss}^{\pm}(x,t) =$ $c_s^{\pm}(x, R_s^{\pm}, t)$, U^{\pm} is the open-circuit potential, and $c_{s, \max}^{\pm}$ is the maximum possible concentration in the solid phase. A complete exposition of the model equations and boundary conditions can be found in [1], [28]. The input to the model is the applied current density I(t) [A/m²], and the output is the voltage measured across the current collectors:

$$V(t) = \phi_s^+(0^+, t) - \phi_s^-(0^-, t). \tag{9}$$

Symbols are defined in Table II of the Appendix. Note the mathematical structure, which contains linear PDEs (1), quasilinear PDEs (2), ODEs in space (3)-(5), and nonlinear algebraic constraints (6)-(8). This presents a formidable task for model-based state of health estimation. Consequently, we seek an appropriately reduced model that maintains prediction fidelity.

B. The Reduced-Order Electrochemical Model

From the previous work [14], the reduced-order model and associated state estimators are derived with the following assumptions:

- [A1]: The solid phase Li concentration in each electrode is constant in the spatial coordinate x, uniformly in time. Mathematically, $c_s^{\pm}(x,r,t)$ and $j_n^{\pm}(x,t)$ are constant in
- [A2]: The exchange current density term $i_0^{\pm}(x,t)$ can be approximated by its averaged value $\bar{i}_0^{\pm}(t)$, which is independent of x.
- [A3]: The constants $\alpha_a = \alpha_c$ (hereafter denoted simply
- by α). This assumption is almost always true in practice. [A4]: The term $k_f(x,t) \doteq \left(1 + \frac{d \ln f_{c/a}}{d \ln c_e}(x,t)\right)$ is approximately constant in x, i.e. $\bar{k}_f(t) \approx k_f(x,t)$.
- [A5]: The term $\kappa(c_e)$ is approximately constant in c_e , i.e. $\overline{\kappa} \approx \kappa(c_e)$.
- [A6]: The total moles of lithium in the electrolyte $n_{Li,e}$ and in the solid phase $n_{Li,s}$ are both conserved.
- [A7]: The total moles of lithium in the solid phase, $n_{\rm Li.s}$ in (23), is known beforehand for state observer design.
- [A8]: The total moles of lithium in the electrolyte, $n_{\rm Li,e}$ in (24), is known beforehand for state observer design.

These assumptions ultimately render a model consisting of: (i) two linear spherical diffusion PDEs modeling each electrode's solid concentration dynamics, (ii) a quasilinear diffusion equation (across three domains) modeling the electrolyte concentration dynamics, and (iii) a nonlinear output function mapping boundary values of solid concentration, electrolyte concentration, and current to voltage.

In this work, we aim to relax some of these assumptions in order to improve the model fidelity and state observer performance. The state-dependent parameters are preserved in the model output equation, which removes [A4] - [A5]. Next, the total moles of lithium in the solid-phase and electrolyte-phase are estimated by using sensitivity analysis, which eliminates assumptions [A6] - [A8]. The state-dependent parameters in the electrolyte-phase, i.e. diffusivity, conductivity, and activity coefficients are strongly dependent on the electrolyte concentration. Specifically, they vary by an order of magnitude [29] with c_e . Hence, it is of great importance to incorporate statedependent electrochemical parameters, which is shown to have a greater impact on voltage prediction under high current.

To begin, applying assumptions [A1]-[A3] removes the spatial dependence of a variable, and thus an overline is added to the variable name to avoid confusion. The first step is to combine [A1] and ODE (5) to express molar ion flux as proportional to current,

$$\bar{j}_n^+(t) = -\frac{I(t)}{Fa^+L^+}, \qquad \bar{j}_n^-(t) = \frac{I(t)}{Fa^-L^-}.$$
 (10)

Note that the ionic current $i_e(x,t)$ has the trapezoidal shape [14]. Apply \overline{j}_n^{\pm} in (10) to the solid-phase diffusion equations and boundary conditions:

$$\frac{\partial \overline{c}_{s}^{\pm}}{\partial t}(r,t) = \frac{1}{r^{2}} \frac{\partial}{\partial r} \left[D_{s}^{\pm} r^{2} \frac{\partial \overline{c}_{s}^{\pm}}{\partial r}(r,t) \right], \qquad (11)$$

$$\frac{\partial \overline{c}_{s}^{\pm}}{\partial r}(0,t) = 0, \quad \frac{\partial \overline{c}_{s}^{\pm}}{\partial r}(R_{s}^{\pm},t) = \pm \frac{1}{D_{s}^{\pm} F a^{\pm} L^{\pm}} I(t).$$

Next, we derive the electrolyte diffusion equations by combining PDE (2) with (5), (10), and [A1]:

$$\frac{\partial c_e^-}{\partial t}(x,t) = \frac{\partial}{\partial x} \left[D_e(c_e^-) \frac{\partial c_e^-}{\partial x}(x,t) \right] + \frac{(1-t_c^0)}{\varepsilon_e^- F L^-} I(t), \quad (12)$$

$$\frac{\partial c_e^{\text{sep}}}{\partial t}(x,t) = \frac{\partial}{\partial x} \left[D_e(c_e^{\text{sep}}) \frac{\partial c_e^{\text{sep}}}{\partial x}(x,t) \right], \quad (13)$$

$$\frac{\partial c_e^+}{\partial t}(x,t) = \frac{\partial}{\partial x} \left[D_e(c_e^+) \frac{\partial c_e^+}{\partial x}(x,t) \right] - \frac{(1-t_c^0)}{\varepsilon_e^+ F L^+} I(t).$$
(14)

Note that the boundary conditions are the same as the fullorder model. Next, we derive the nonlinear output function for terminal voltage, which is distinguished from previous work. From (9), we notice the voltage V(t) depends on the solid potential at the current collectors $\phi_s^{\pm}(x,t)$. Therefore, we solve (8) in terms of ϕ_s and spatially averaged quantities,

$$\phi_s^{\pm}(x,t) = \bar{\eta}^{\pm}(t) + \phi_e^{\pm}(x,t) + U^{\pm}(\bar{c}_{ss}^{\pm}(t)) + FR_f^{\pm}\bar{j}_n^{\pm}(t). \tag{15}$$

Next we derive each term on the right hand side of (15). Overpotential $\bar{\eta}^{\pm}(t)$ is found by solving the Butler-Volmer equation (6) in terms of $\bar{\eta}^{\pm}(t)$, applying [A1], [A2], [A4], and substituting (10),

$$\bar{\eta}^{\pm}(t) = \frac{RT}{\alpha F} \sinh^{-1} \left(\frac{\mp I(t)}{2a^{\pm} L^{\pm} \bar{i}_0^{\pm}(t)} \right). \tag{16}$$

The electrolyte potential $\phi_e^{\pm}(x,t)$ is found by integrating ODE (4) w.r.t. x across the entire cell width,

$$\int_{0^{-}}^{0^{+}} \frac{\partial \phi_{e}}{\partial x}(x,t)dx = \int_{0^{-}}^{0^{+}} \frac{-i_{e}^{\pm}(x,t)}{\kappa(c_{e}(x,t))} dx + \int_{0^{-}}^{0^{+}} \frac{2RT}{F} (1 - t_{c}^{0}) \times \left(1 + \frac{d \ln f_{c/a}}{d \ln c_{e}}(x,t)\right) \frac{\partial \ln c_{e}}{\partial x}(x,t) dx.$$
(17)

Note that previous work [14] assumed c_e -dependent parameters such as conductivity, $\kappa(c_e)^1$ and activity coefficient,

¹The superscript {eff} is dropped in the notation for readability

 $\frac{d \ln f_{c/a}}{d \ln c_e}(x,t)$ in **[A4], [A5]** are constant in c_e . With the trapezoidal shape of ionic current, the first term in (17) can be expressed as:

$$\phi_e^{+}(0^+,t) - \phi_e^{-}(0^-,t) = \frac{-I(t)}{L^{-}} \int_{0^-}^{L^{-}} \frac{x}{\kappa(c_e(x,t))} dx$$
$$-I(t) \int_{L^{-}}^{L^{sep}} \frac{1}{\kappa(c_e(x,t))} dx + \frac{I(t)}{L^{+}} \int_{L^{sep}}^{0^+} \frac{x - 0^+}{\kappa(c_e(x,t))} dx$$
$$+ \int_{0^-}^{0^+} \frac{2RT}{F} (1 - t_c^0) \times \left(1 + \frac{d \ln f_{c/a}}{d \ln c_e}(x,t) \right) \frac{\partial \ln c_e}{\partial x}(x,t) dx.$$
(18)

Note that the activity coefficient is present in the anode, separator, and cathode respectively. We introduce $\kappa_A(c_e(x,t))=1+\frac{d\ln f_{c/a}}{d\ln c_e}(x,t)$ for simplicity,

$$\phi_{e}^{+}(0^{+},t) - \phi_{e}^{-}(0^{-},t) = \frac{-I(t)}{L^{-}} \int_{0^{-}}^{L^{-}} \frac{x}{\kappa(c_{e}(x,t))} dx$$

$$-I(t) \int_{L^{-}}^{L^{sep}} \frac{1}{\kappa(c_{e}(x,t))} dx + \frac{I(t)}{L^{+}} \int_{L^{sep}}^{0^{+}} \frac{x - 0^{+}}{\kappa(c_{e}(x,t))} dx$$

$$+ \frac{2RT}{F} (1 - t_{c}^{0}) \left[\int_{0^{-}}^{L^{-}} \kappa_{A}(c_{e}(x,t)) \frac{\partial \ln c_{e}}{\partial x}(x,t) dx \right]$$

$$+ \int_{L^{-}}^{L^{sep}} \kappa_{A}(c_{e}(x,t)) \frac{\partial \ln c_{e}}{\partial x}(x,t) dx$$

$$+ \int_{L^{sep}}^{L^{+}} \kappa_{A}(c_{e}(x,t)) \frac{\partial \ln c_{e}}{\partial x}(x,t) dx \right].$$
(19)

Using integration by parts, $\int f(x)g'(x)dx = f(x)g(x) - \int f'(x)g(x)dx$ and chain rule provides the following algebra,

$$\phi_{e}^{+}(0^{+},t) - \phi_{e}^{-}(0^{-},t) = \frac{-I(t)}{L^{-}} \int_{0^{-}}^{L^{-}} \frac{x}{\kappa(c_{e}(x,t))} dx$$

$$-I(t) \int_{L^{-}}^{L^{sep}} \frac{1}{\kappa(c_{e}(x,t))} dx + \frac{I(t)}{L^{+}} \int_{L^{sep}}^{0^{+}} \frac{x - 0^{+}}{\kappa(c_{e}(x,t))} dx$$

$$+ \frac{2RT}{F} (1 - t_{c}^{0}) \left[\kappa_{A}(c_{e}(x,t)) \ln c_{e}(x,t) \Big|_{x=0^{-}}^{x=L^{-}} \right.$$

$$- \int_{c_{e}(0^{-},t)}^{c_{e}(L^{-},t)} \kappa'_{A}(c_{e}(x,t)) \ln c_{e}(x,t) dc_{e}(x,t)$$

$$+ \kappa_{A}(c_{e}(x,t)) \ln c_{e}(x,t) dc_{e}(x,t)$$

$$- \int_{c_{e}(L^{-},t)}^{c_{e}(L^{sep},t)} \kappa'_{A}(c_{e}(x,t)) \ln c_{e}(x,t) dc_{e}(x,t)$$

$$+ \kappa_{A}(c_{e}(x,t)) \ln c_{e}(x,t) dc_{e}(x,t)$$

$$- \int_{c_{e}(L^{sep},t)}^{c_{e}(L^{+},t)} \kappa'_{A}(c_{e}(x,t)) \ln c_{e}(x,t) dc_{e}(x,t) \right].$$

$$(20)$$

We simply denote the electrolyte potential difference (20) by $\Delta\Phi_e(c_e(x,t),\kappa(c_e(x,t)),\kappa_A(c_e(x,t)),I(t))$. We write the voltage output for the SPMe model as:

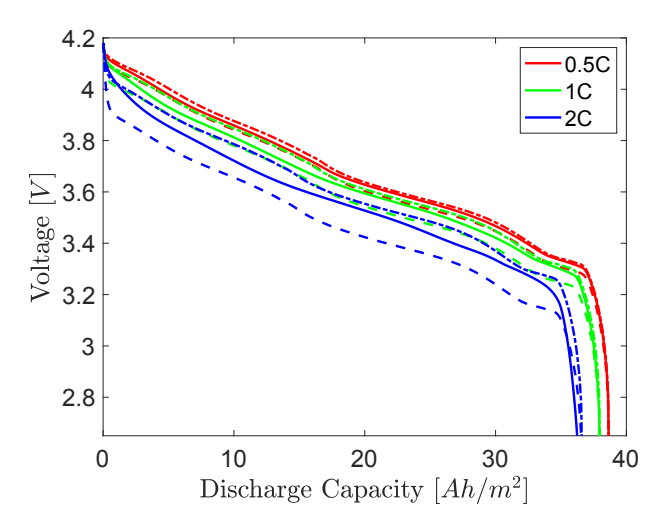


Figure 2: The comparison of proposed SPMe(-.) with DFN(-) and previous SPMe(- -) model [14] for NCA electrochemical parameters identified in [7].

| | 0.5C | 1C | 2C |
|---------------|---------|---------|---------|
| Proposed SPMe | 16.1 mV | 29.6 mV | 46.5 mV |
| SPMe [14] | 19.4 mV | 40.3 mV | 87.6 mV |

Table I: The output voltage error with respect to DFN model.

$$V(t) = \frac{RT}{\alpha F} \sinh^{-1} \left(\frac{-I(t)}{2a^{+}L^{+}\bar{i}_{0}^{+}(t)} \right)$$

$$- \frac{RT}{\alpha F} \sinh^{-1} \left(\frac{I(t)}{2a^{-}L^{-}\bar{i}_{0}^{-}(t)} \right)$$

$$+ U^{+}(\bar{c}_{ss}^{+}(t)) - U^{-}(\bar{c}_{ss}^{-}(t)) - \left(\frac{R_{f}^{+}}{a^{+}L^{+}} + \frac{R_{f}^{-}}{a^{-}L^{-}} \right) I(t)$$

$$+ \Delta \Phi_{e} \left(c_{e}(x,t), \kappa(c_{e}(x,t)), \kappa_{A}(c_{e}(x,t)), I(t) \right). \tag{21}$$

The terminal voltage output equation can be described as a combination of electrochemical differences between two electrodes and the electrolyte,

$$V(t) = \Delta U(\bar{c}_{ss}^{\pm}) + \Delta \phi_e(c_e, I) + \Delta \bar{\eta}(\bar{c}_{ss}^{\pm}, I) - \left(\frac{R_f^+}{a^+ L^+} + \frac{R_f^-}{a^- L^-}\right) I(t).$$
 (22)

We validate the proposed SPMe model with the full-order model identified in previous work [14] by comparing the voltage prediction accuracy. A 18650 Lithium nickel-cobalt-aluminum oxide (NCA) battery parameters identified previous work [7] are adopted to simulate the electrochemcial models. Suppose the DFN model represents a truth battery model. We visualize the voltage predictions with different C-rates in Fig 2. The proposed model (-.) outperforms the previous work (--) compared to the truth model (-) in terms of voltage. The quantitative analysis for the voltage comparison is summarized in Table I. The voltage root mean square error (RMSE) is computed up to 80 % of discharge capacity. We emphasize the inclusion of the state-dependent electrolyte parameters are

critical to the model-order-reduction, as they are shown in the output voltage equation (21) directly. Furthermore, the voltage output is strongly affected by the electrolyte characteristics of the cell. For instance, the conventional SPMe model has lower voltage prediction error for the Lithium cobalt oxide (LiCoO₂) chemistry in [14]. However, the prediction gets worse for the NCA chemistry in [7].

C. The State of Health (SOH) for Electrochemical Model

In this paper, we focus on *the moles of lithium* in the solid phase and electrolyte phase, which impact Li-ion battery state of health (SOH). They are defined as:

$$n_{Li,s}(t) = \sum_{j \in \{+,-\}} \frac{\varepsilon_s^j L^j A}{\frac{4}{3}\pi (R_s^j)^3} \int_0^{R_s^j} 4\pi r^2 c_s^j(r,t) dr.$$
 (23)

$$n_{Li,e}(t) = \sum_{j \in \{-,sep,+\}} \varepsilon_e^j A \int_{0^j}^{L^j} c_e^j(x,t) dx.$$
 (24)

These quantities are initially determined during the manufacturing process by the Li metal in the active materials and lithium ions dissolved in the electrolyte. In realistic scenarios, the moles of lithium are not conserved due to aging mechanisms, e.g. SEI layer growth, Li-plating, and solvent oxidation. The loss of total lithium contained in the solid phase is known to cause capacity fade, and the loss of total lithium in the electrolyte phase contributes to power fade. Figure 3 illustrates this phenomenon, where we have reduced the amount of cyclable lithium for each phase. The moles of lithium is decreased by 10% to represent an aged cell, and compared with the fresh cell in simulation. Mathematically, these changes only affect the initial conditions of the electrochemical states. The battery is fully discharged to the minimum voltage threshold using constant current in order to analyze the capacity fade in Fig. 3a, while high C-rate pulse current is applied to the battery for power fade demonstration in Fig. 3b. We observe that the moles of lithium contribute to degrading state of health in Liion batteries. Note that the change of $n_{Li,s}$ affects the initial conditions of solid-phase concentration, $c_s(r,0)$ while the perturbation of $n_{Li,e}$ directly impacts the initial conditions of electrolyte concentration, $c_e(x,0)$.

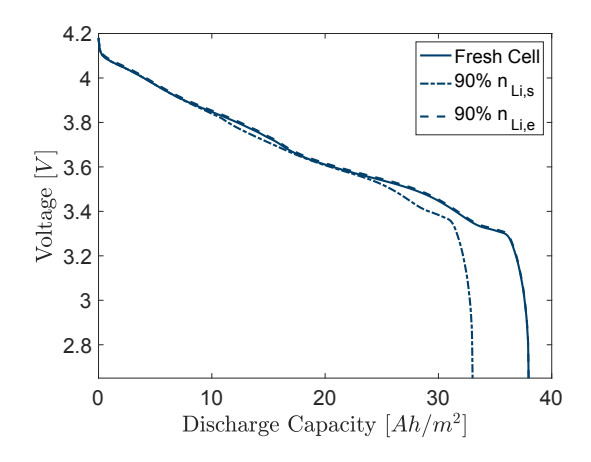
In order to estimate these SOH parameters, we first combine the system dynamics (11) - (14) with the algebraic equations (23) - (24), which results in the differential algebraic equations (DAEs),

$$\dot{\boldsymbol{x}} = \boldsymbol{f}(\boldsymbol{x}, \boldsymbol{z}, u), \quad \boldsymbol{x}(t_0) = \mathbf{x_0}, \tag{25}$$

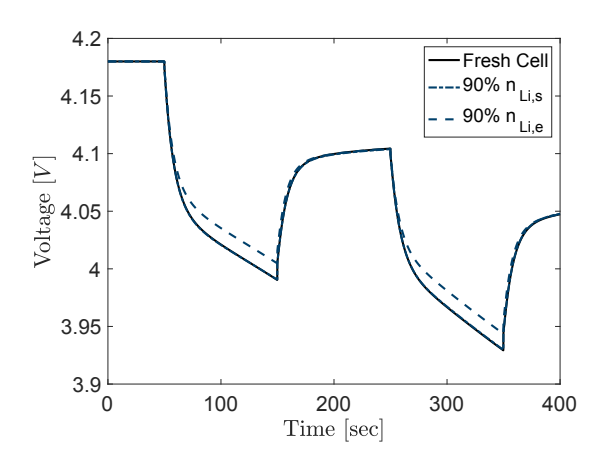
$$\mathbf{0} = \boldsymbol{g}(\boldsymbol{x}, \boldsymbol{z}, u), \quad \boldsymbol{z}(t_0) = \mathbf{z_0}, \tag{26}$$

$$\mathbf{y} = \boldsymbol{h}(\boldsymbol{x}, \boldsymbol{z}, \boldsymbol{u}),\tag{27}$$

after discretizing (11) – (14) and (23) – (24) in space via a suitable methods, e.g. finite differences, Padé approximation, spectral methods, etc. [30], [31]. Denote $\mathbf{x} = [c_s^-, c_s^+, c_e]^T \in \mathbb{R}^{n_x}$ as state vectors, $\mathbf{z} = [n_{\text{Li},s}, n_{\text{Li},e}]^T \in \mathbb{R}^{n_z}$ as algebraic variables, $\mathbf{y} = V(t)$ as output variable defined in (21). The system is a semi-explicit DAE of index 1 as $[\partial \mathbf{g}/\partial \mathbf{z}]^{-1}$ exists and the SOH parameters, \mathbf{z} , only appear in the initial conditions of time-derivative states \mathbf{x}_0 .



(a) 1C Constant Current Discharge.



(b) 2C Pulse Current Discharge.

Figure 3: The impact of SOH parameters $n_{Li,s}$, $n_{Li,e}$ on voltage output. Top: A decrease of $n_{Li,s}$ decreases capacity, i.e., capacity fade. Bottom: a decrease of $n_{Li,e}$ affects the instantaneous voltage, which contributes to power fade.

III. SOH PARAMETER ESTIMATION

This section derives estimators for SOH parameters $n_{Li,s}$, $n_{Li,e}$ by leveraging the proposed SPMe model in Section II and (25)-(27).

A. Sensitivity Analysis

Sensitivity analysis is used to understand how a model's output depends on variations in parameter values, or initial conditions [7]. For time-continuous dynamic systems, the local sensitivities are defined as the first-order partial derivatives of the system output with respect to the parameters around nominal parameter values. In this section, we briefly introduce how to derive local sensitivity of SOH parameters in dynamical system described in (25)-(27), and develop this approach toward an SOH parameter estimation framework.

Let's define sensitivity variables as follows:

$$S_{\mathbf{x}} = \frac{\partial \mathbf{x}}{\partial \mathbf{z}}, \quad S_{\mathbf{y}} = \frac{\partial \mathbf{y}}{\partial \mathbf{z}},$$
 (28)

where $S_{\mathbf{x}}$ and $S_{\mathbf{y}}$ are sensitivity matrices of the local sensitivity vector where $s_{i,j}$ is defined as the partial derivative of the i-th state to the j-th algebraic variable such as:

$$s_{i,j}(t) = \frac{\partial x_i(t)}{\partial z_j}. (29)$$

Then, we can formulate the sensitivity differential equations (SDEs) for the system (25) – (27) via multivariate calculus as follows:

$$\dot{S}_{\mathbf{x}} = \frac{\partial \mathbf{f}}{\partial \mathbf{x}} \cdot S_{\mathbf{x}} + \frac{\partial \mathbf{f}}{\partial \mathbf{z}}, \quad S_{\mathbf{x}}(0) = S_{\mathbf{x}0},$$
 (30)

$$S_{\mathbf{y}} = \frac{\partial \mathbf{h}}{\partial \mathbf{x}} \cdot S_{\mathbf{x}} + \frac{\partial \mathbf{z}}{\partial \mathbf{z}}, \quad S_{\mathbf{y}}(0) = S_{\mathbf{y}0}, \tag{31}$$

$$0 = \frac{\partial \mathbf{g}}{\partial \mathbf{x}} \cdot S_{\mathbf{x}}(0) + \frac{\partial \mathbf{g}}{\partial \mathbf{z}}.$$
 (32)

Note that the sensitivity dynamic equations are formulated as ordinary differential equations (ODEs), not differential algebraic equations (DAEs) because the sensitivity vectors are obtained by differentiating the states and outputs with respect to the algebraic variables. It is important to notice that the algebraic equations (32) are only used for sensitivity initial conditions, $S_{\mathbf{x}}(0)$ as the algebraic variables only appear in the initial conditions of the states in (26). The advantage of SDEs lies in fundamental mathematical derivation and computational efficiency compared to a perturbation method whose sensitivity is obtained by perturbing each parameter slightly, finding the corresponding initial conditions, and then calculating the output difference with nominal parameters. Notice that SDEs are time-varying ODEs where Jacobians of state transition functions, algebraic equations with respect to the states, and algebraic variables should be computed at each time step. Such intricate ODEs encourage researchers to utilize automatic differentiation tools, such as CasADi [32], which efficiently computes the first and second-order derivatives of this intricate model. In this work, the battery model DAEs and its SDEs are simulated by using the IDAS/CVODES integrator provided by SUNDIALS via CasADi interfaces [33].

B. Nonlinear Least Squares

In this subsection, we will use the sensitivity results from the preceding section to estimate the SOH parameters. This estimation problem can be formulated as a nonlinear optimization problem, i.e., nonlinear least squares. The objective is to minimize the output voltage difference between measured output, y, and predicted output, \hat{y} :

$$\min_{\hat{z}} \cdot \sum_{t=0}^{t_f} [\mathbf{y}(t) - \hat{\mathbf{y}}(t; \hat{z})]^2.$$
 (33)

The Levenberg-Marquardt algorithm is used to update the parameters \hat{z} iteratively by solving the nonlinear optimization problem (33) above. This algorithm adaptively chooses parameter updates between the gradient descent update and the Gauss-Newton update [34] via equation:

$$\left[\mathbf{J}^{T}\mathbf{J} + \gamma \operatorname{diag}(\mathbf{J}^{T}\mathbf{J})\right] h_{\hat{z}} = \mathbf{J}^{T}(\mathbf{y} - \hat{\mathbf{y}}), \tag{34}$$

where $\mathbf{J} = \partial \hat{\mathbf{y}}/\partial \hat{\mathbf{z}}$ is the local sensitivity of the output $\hat{\mathbf{y}}$, which is equivalent to the sensitivity vector, $S_{\mathbf{v}}$ from (30) – (32). The value of γ trades off between gradient descent update and Gauss-Newton update. Then the parameters are updated iteratively by

$$\hat{z}_{k+1} = \hat{z}_k + h_{\hat{z}}. (35)$$

Once the parameters are fit to the data, the least squares estimator provides the parameter estimation statistics evaluated at the final estimates denoted by \underline{z} . Namely,

$$\hat{\mathbf{z}} \sim \mathcal{N}\left(\underline{\mathbf{z}}, \hat{\rho}^2(\underline{\mathbf{z}})\right),$$
 (36)

the confidence intervals are obtained via t-distribution because the standard deviation is unknown [35]. The estimated covariance is computed as:

$$\hat{\rho}^2(\underline{z}) = \hat{\sigma}^2 \left[\mathbf{J}(\underline{z})^T \mathbf{J}(\underline{z}) \right]^{-1}, \tag{37}$$

where J(z) is the local sensitivity at the final estimates. The error variance σ^2 is introduced to make the estimator unbiased such as:

$$\hat{\sigma}^2 = \frac{1}{N - p} \sum_{t=0}^{t_f} \left[\mathbf{y}(t) - \hat{\mathbf{y}}(t; \underline{z}) \right]^2, \tag{38}$$

where N is the number of observations and p is the number of parameters. The 95 % confidence intervals are derived by using t-distributions:

$$\underline{z} - t_{(1-0.025)} \frac{\hat{\rho}}{\sqrt{N}} \le z^* \le \underline{z} + t_{(1-0.025)} \frac{\hat{\rho}}{\sqrt{N}}, \quad (39)$$

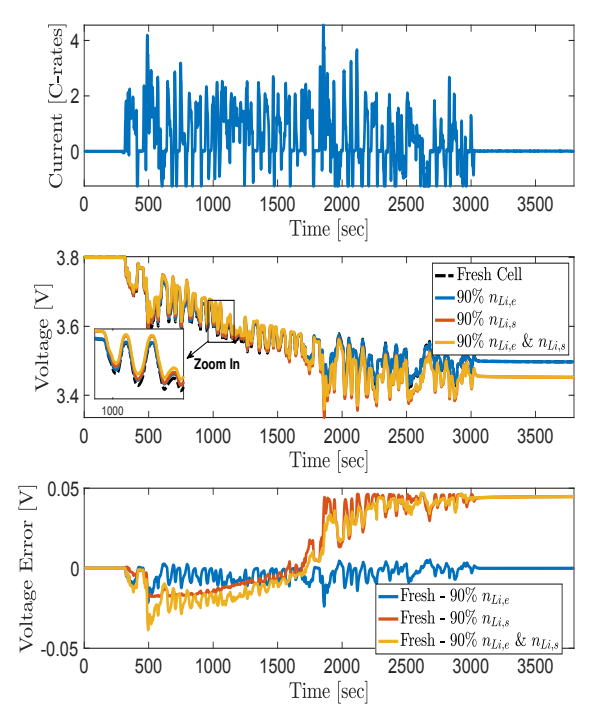
where t is the upper critical value for the t-distribution with N-1 freedom [35], [36].

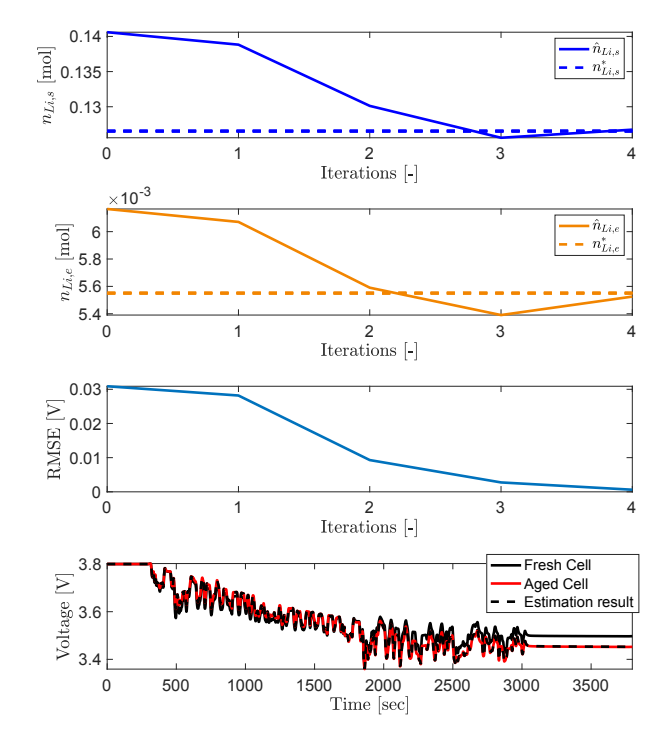
IV. SIMULATION RESULTS

In this section, we present SOH parameter estimation results to validate the proposed approach via simulation. Suppose the aging mechanisms consume moles of lithium in solid and electrolyte phase after a number of cycles. Then the voltage starts to deviate compared to a fresh cell. Even though the exact underlying ageing mechanisms are not considered in this study, many of them ultimately lead to a decrease of these quantities. Our goal is to track these SOH parameters by nonlinear least squares using input/output measurements.

Figure 4a exhibits the impact of parameter changes to the output voltage. The Urban Dynamometer Driving Schedule (UDDS) input profile is considered as an input current profile applied to the enhanced SPMe. We compare the voltage deviations of the proposed SPMe with different SoH parameter values. One can notice that the perturbation of $n_{Li,s}$ affects the voltage variation in the whole period even after cycling, i.e. the relaxation period. This is because $n_{Li,s}$ is related to the equilibrium structure of the electrochemical model determining the window of the open-circuit voltage (OCV) curve [7]. Consequently, a change of $n_{Li,s}$ shifts the equilibrium states during the relaxation period. On the other hand, the $n_{Li,e}$ parameter is linked to the electrolyte concentrations by definition. This fact implies that a change

of $n_{Li,e}$ influences on the level of electrolyte concentration,





- (a) The voltage output error between fresh cell and aged cell.
- (b) The SOH parameter estimation results.

Figure 4: The simulation results on the voltage deviations as well as SOH estimation using Urban Dynamometer Driving Schedule (UDDS) input profile. The voltage RMSE reduces below 1 mV after 4 iterations using Levenberg-Marquardt algorithm.

which alters the instantaneous voltage output during operation. Interestingly, $n_{Li,s}$ and $n_{Li,e}$ are linearly independent with each other, with respect to the output voltage variation since they shown up in separate terms of (22). We confirm that the voltage errors are linearly independent at the bottom in Fig. 4a. For instance, the voltage error (Verr) is linearly independent on each other, $\operatorname{Verr}(90\%\,n_{Li,s}\&90\%\,n_{Li,e}) = \operatorname{Verr}(90\%\,n_{Li,s}) + \operatorname{Verr}(90\%\,n_{Li,e})$. This fact makes the SOH parameter estimation problem simpler and straightforward.

In these simulations, we adopt the electrochemical parameters for a fresh cell identified in the authors' previous work [7]. Specifically, the "true" SOH parameters are set as $n_{Li,s}=0.1406$ [mol], $n_{Li,e}=0.0062$ [mol]. To represent the aged cell behavior, we assume that the aged cell retains 90 % moles from the fresh cell, i.e., $n_{Li,s}=0.1265$ [mol], $n_{Li,e}=0.0056$ [mol]. The parameter updates at each iteration compared to the true parameters (aged) are shown at the top in Fig. 4b. Note that the parameter estimation is a batch process where the voltage RMSE decreases every iteration by updating the SOH parameters. After 4 iterations the parameter estimates approach the correct aged cell values. Moreover, the voltage RMSE reaches less than 1 mV. The final parameter estimates with 95% confidence interval are obtained as $\hat{n}_{Li,s}=0.1267\pm2.09\times10^{-5}$ [mol], and $\hat{n}_{Li,e}=0.0055\pm7.80\times10^{-6}$ [mol].

V. CONCLUSIONS

This paper addresses state-of-health (SOH) parameter identification for an electrochemical battery model. The fidelity of the single particle model with electrolyte (SPMe) is improved by taking the state-dependent parameters into account in the

output voltage equation. We consider the SOH estimation problem for general electrochemical models, and propose a parameter estimation framework via sensitivity analysis. Once the output voltage measurement starts to diverge from the fresh cell behavior due to ageing mechanisms, the Levenberg-Marquardt algorithm is used to solve a nonlinear least squares problem for SOH parameter fitting. In order to validate our proposed framework, we simulate the overall process using a model-to-model comparison. These results demonstrate how the SOH parameters are monitored by proposed approach. Ongoing work involves validation of the proposed SOH parameter estimation framework with experimental data.

REFERENCES

- N. A. Chaturvedi, R. Klein, J. Christensen, J. Ahmed, and A. Kojic, "Algorithms for advanced battery-management systems," *IEEE Control systems magazine*, vol. 30, no. 3, pp. 49–68, 2010.
- [2] M. A. Hannan, M. H. Lipu, A. Hussain, and A. Mohamed, "A review of lithium-ion battery state of charge estimation and management system in electric vehicle applications: Challenges and recommendations," *Renewable and Sustainable Energy Reviews*, vol. 78, pp. 834–854, 2017.
- [3] X. Hu, S. Li, and H. Peng, "A comparative study of equivalent circuit models for li-ion batteries," *Journal of Power Sources*, vol. 198, pp. 359–367, 2012.
- [4] M. Doyle, T. F. Fuller, and J. Newman, "Modeling of galvanostatic charge and discharge of the lithium/polymer/insertion cell," *Journal of the Electrochemical Society*, vol. 140, no. 6, pp. 1526–1533, 1993.
- [5] D. Di Domenico, A. Stefanopoulou, and G. Fiengo, "Lithium-ion battery state of charge and critical surface charge estimation using an electrochemical model-based extended kalman filter," *Journal of dynamic* systems, measurement, and control, vol. 132, no. 6, 2010.
- [6] D. Zhang, S. Dey, L. D. Couto, and S. J. Moura, "Battery adaptive observer for a single-particle model with intercalation-induced stress," *IEEE transactions on control systems technology*, 2019.

- [7] S. Park, D. Kato, Z. Gima, R. Klein, and S. Moura, "Optimal experimental design for parameterization of an electrochemical lithium-ion battery model," *Journal of The Electrochemical Society*, vol. 165, no. 7, p. A1309, 2018.
- [8] Q. Lai, S. Jangra, H. J. Ahn, G. Kim, W. T. Joe, and X. Lin, "Analytical derivation and analysis of parameter sensitivity for battery electrochemical dynamics," *Journal of Power Sources*, vol. 472, p. 228338, 2020.
- [9] S. Santhanagopalan and R. E. White, "Online estimation of the state of charge of a lithium ion cell," *Journal of power sources*, vol. 161, no. 2, pp. 1346–1355, 2006.
- [10] Y. Yin, Y. Hu, S.-Y. Choe, H. Cho, and W. T. Joe, "New fast charging method of lithium-ion batteries based on a reduced order electrochemical model considering side reaction," *Journal of Power Sources*, vol. 423, pp. 367–379, 2019.
- [11] S. Dey, B. Ayalew, and P. Pisu, "Nonlinear adaptive observer for a lithium-ion battery cell based on coupled electrochemical-thermal model," *Journal of Dynamic Systems, Measurement, and Control*, vol. 137, no. 11, 2015.
- [12] S.-X. Tang, L. Camacho-Solorio, Y. Wang, and M. Krstic, "State-of-charge estimation from a thermal–electrochemical model of lithium-ion batteries," *Automatica*, vol. 83, pp. 206–219, 2017.
- [13] S. G. Marquis, V. Sulzer, R. Timms, C. P. Please, and S. J. Chapman, "An asymptotic derivation of a single particle model with electrolyte," *Journal of The Electrochemical Society*, vol. 166, no. 15, p. A3693, 2019
- [14] S. J. Moura, F. B. Argomedo, R. Klein, A. Mirtabatabaei, and M. Krstic, "Battery state estimation for a single particle model with electrolyte dynamics," *IEEE Transactions on Control Systems Technology*, vol. 25, no. 2, pp. 453–468, 2016.
- [15] T. R. Tanim, C. D. Rahn, and C.-Y. Wang, "A temperature dependent, single particle, lithium ion cell model including electrolyte diffusion," *Journal of Dynamic Systems, Measurement, and Control*, vol. 137, no. 1, 2015
- [16] T. R. Tanimm, C. D. Rahn, and C.-Y. Wang, "State of charge estimation of a lithium ion cell based on a temperature dependent and electrolyte enhanced single particle model," *Energy*, vol. 80, pp. 731–739, 2015.
- [17] C. R. Birkl, M. R. Roberts, E. McTurk, P. G. Bruce, and D. A. Howey, "Degradation diagnostics for lithium ion cells," *Journal of Power Sources*, vol. 341, pp. 373–386, 2017.
- [18] X. Lin, J. Park, L. Liu, Y. Lee, A. Sastry, and W. Lu, "A comprehensive capacity fade model and analysis for li-ion batteries," *Journal of The Electrochemical Society*, vol. 160, no. 10, p. A1701, 2013.
- [19] J. Christensen and J. Newman, "Effect of anode film resistance on the charge/discharge capacity of a lithium-ion battery," *Journal of the Electrochemical Society*, vol. 150, no. 11, p. A1416, 2003.
- [20] S. Santhanagopalan, Q. Zhang, K. Kumaresan, and R. E. White, "Parameter estimation and life modeling of lithium-ion cells," *Journal of The Electrochemical Society*, vol. 155, no. 4, p. A345, 2008.
- [21] S. Lee, J. Kim, J. Lee, and B. H. Cho, "State-of-charge and capacity estimation of lithium-ion battery using a new open-circuit voltage versus state-of-charge," *Journal of power sources*, vol. 185, no. 2, pp. 1367– 1373, 2008.
- [22] C. Hu, B. D. Youn, and J. Chung, "A multiscale framework with extended kalman filter for lithium-ion battery soc and capacity estimation," *Applied Energy*, vol. 92, pp. 694–704, 2012.
- [23] D. Zhang, S. Dey, H. E. Perez, and S. J. Moura, "Real-time capacity estimation of lithium-ion batteries utilizing thermal dynamics," *IEEE Transactions on Control Systems Technology*, vol. 28, no. 3, pp. 992–1000, 2019.
- [24] S. J. Moura, N. A. Chaturvedi, and M. Krstić, "Adaptive partial differential equation observer for battery state-of-charge/state-of-health estimation via an electrochemical model," *Journal of Dynamic Systems, Measurement, and Control*, vol. 136, no. 1, p. 011015, 2014.
- [25] X. Zhou, J. L. Stein, and T. Ersal, "Battery state of health monitoring by estimation of the number of cyclable li-ions," *Control Engineering Practice*, vol. 66, pp. 51–63, 2017.
- [26] M. Huang, M. Kumar, C. Yang, and A. Soderlund, "Aging estimation of lithium-ion battery cell using an electrochemical model-based extended kalman filter," in AIAA Scitech 2019 Forum, 2019, p. 0785.
- [27] W. Van Schalkwijk and B. Scrosati, "Advances in lithium ion batteries
- [28] K. E. Thomas, J. Newman, and R. M. Darling, "Mathematical modeling of lithium batteries," in *Advances in lithium-ion batteries*. Springer, 2002, pp. 345–392.

- introduction," in *Advances in Lithium-Ion Batteries*. Springer, 2002, pp. 1–5.
- [29] L. O. Valøen and J. N. Reimers, "Transport properties of lipf6-based li-ion battery electrolytes," *Journal of The Electrochemical Society*, vol. 152, no. 5, p. A882, 2005.
- [30] J. C. Forman, S. Bashash, J. L. Stein, and H. K. Fathy, "Reduction of an electrochemistry-based li-ion battery model via quasi-linearization and pade approximation," *Journal of the Electrochemical Society*, vol. 158, no. 2, pp. A93–A101, 2011.
- [31] G. Fan, K. Pan, and M. Canova, "A comparison of model order reduction techniques for electrochemical characterization of lithium-ion batteries," in *Decision and Control (CDC)*, 2015 IEEE 54th Annual Conference on. IEEE, 2015, pp. 3922–3931.
- [32] J. Andersson, "A General-Purpose Software Framework for Dynamic Optimization," PhD thesis, Arenberg Doctoral School, KU Leuven, Department of Electrical Engineering (ESAT/SCD) and Optimization in Engineering Center, Kasteelpark Arenberg 10, 3001-Heverlee, Belgium, October 2013.
- [33] A. C. Hindmarsh, P. N. Brown, K. E. Grant, S. L. Lee, R. Serban, D. E. Shumaker, and C. S. Woodward, "Sundials: Suite of nonlinear and differential/algebraic equation solvers," ACM Transactions on Mathematical Software (TOMS), vol. 31, no. 3, pp. 363–396, 2005.
- [34] K. Levenberg, "A method for the solution of certain non-linear problems in least squares," *Quarterly of applied mathematics*, vol. 2, no. 2, pp. 164–168, 1944.
- [35] D. S. Moore, G. McCabe, and O. Akman, Introduction to the practice of statistics: Continuous random variables. Macmillan, 2005.
- [36] J. A. Rice, Mathematical statistics and data analysis. Cengage Learning, 2006.

Table II: Appendix: Nomenclature

Symbols in order of appearance

| lectrochemical model states, inputs, outputs | | |
|---|--|--|
| | | |
| Lithium concentration in solid phase [mol/m ³] | | |
| Lithium concentration in electrolyte phase [mol/m ³] | | |
| Solid electric potential [V] | | |
| Electrolyte electric potential [V] | | |
| Ionic current [A/m ²] | | |
| Molar ion flux [mol/m ² -s] | | |
| Exchange current density [A/m ²] | | |
| Overpotential [V] | | |
| Lithium concentration at solid particle surface [mol/m ³] | | |
| Total moles of lithium in solid, electrolyte phase [mol] | | |
| Electrode area [m ²] | | |
| Applied current [A/m ²] | | |
| Terminal voltage [V] | | |
| Electrochemical model parameters | | |
| Diffusivity of solid, electrolyte phase [m ² /s] | | |
| Transference number [-] | | |
| Volume fraction of solid, electrolyte phase [-] | | |
| Faraday's constant [C/mol] | | |
| Conductivity of solid $[1/\Omega-m]$ | | |
| Conductivity of electrolyte $[1/\Omega-m]$ | | |
| Universal gas constant [J/mol-K] | | |
| Temperature [K] | | |
| Mean molar activity coefficient in electrolyte [-] | | |
| Specific interfacial surface area [m ² /m ³] | | |
| Anodic, cathodic charge transfer coefficient [-] | | |
| Kinetic reaction rate $[(A/m^2)(mol^3/mol)^{(1+\alpha)}]$ | | |
| Maximum concentration of solid material [mol/m ³] | | |
| Open circuit potential of solid material [V] | | |
| Solid-electrolyte interphase filme resistance $[\Omega$ -m ²] | | |
| Particle radius in solid phase [m] | | |
| Length of region $j \in \{-, \text{sep}, +\}$ | | |
| | | |